

X-ray properties of $z \gtrsim 6.5$ quasars

E. Pons^{1,2*}, R. G. McMahon^{1,2}, M. Banerji^{1,2}, and S. L. Reed³

¹*Institute of Astronomy, University of Cambridge, Madingley Road, Cambridge CB3 0HA, UK*

²*Kavli Institute for Cosmology, University of Cambridge, Madingley Road, Cambridge CB3 0HA, UK*

³*Department of Astrophysical Sciences, Princeton University, 4 Ivy Lane, Princeton, NJ 08544, US*

Accepted XXX. Received YYY; in original form ZZZ

ABSTRACT

We present *XMM-Newton* X-ray observations and analysis of three DES $z > 6.5$ quasars (VDES J0020–3653 at $z = 6.824$, VDES J0244–5008 at $z = 6.724$ and VDES J0224–4711 at $z = 6.526$) and six other quasars with $6.438 < z < 6.747$ from the *XMM-Newton* public archive. Two of the nine quasars are detected at a high ($>4\sigma$) significance level: VDES J0224–4711 ($z=6.53$) at 9σ and PSO J159–02 ($z = 6.38$) at 8σ . They have a photon index of $\Gamma = 1.82^{+0.29}_{-0.27}$ and $\Gamma = 1.94^{+0.31}_{-0.29}$ respectively, which is consistent with the mean value of ~ 1.9 found for quasars at all redshifts. The rest-frame 2–10 keV luminosity of VDES J0224–4711, is $L_{2-10\text{keV}} = (2.92 \pm 0.43) \times 10^{45} \text{ erg s}^{-1}$, which makes this quasar one of the most X-ray luminous quasars at $z > 5.5$ and the most X-ray luminous quasar at $z > 6.5$, with a luminosity 6 times and 2.5 times larger than ULAS J1120+0641 ($z = 7.08$) and ULAS J1342+0928 ($z = 7.54$) respectively. The X-ray-to-optical power-law slopes of the nine quasars are consistent with the previously observed anti-correlation of α_{ox} with UV luminosity $L_{2500\text{\AA}}$. We find no evidence for evolution of α_{ox} with redshift when the anti-correlation with UV luminosity is taken into account. Similar to previous studies at $z \sim 6$ we have found remarkably consistent X-ray spectral properties between low ($z \sim 1$) and high-redshift quasars. Our results add further evidence to the picture that the observable properties of high luminosity quasars over the UV to X-ray spectral region have not evolved significantly from $z \sim 7$ to the present day and that quasars comparable to local versions existed 800 million years after the big bang.

Key words: dark ages – reionisation – galaxies: active – galaxies: high redshift – X-rays: galaxies

1 INTRODUCTION

High-redshift quasars with $z \gtrsim 6.5$ are important probes of the Universe during the epoch of Reionization providing information about the formation, growth and evolution of supermassive black holes (SMBH) and their host galaxies: indeed the presence of $10^9 M_{\odot}$ at $z > 6.5$, 800 million years after the big bang is a challenge for models of black-hole formation and growth (Volonteri 2010; Alexander & Natarajan 2014; Trakhtenbrot et al. 2017). In the last decade, about 30 $z \gtrsim 6.5$ quasars have been discovered mainly from large-area optical and near-infrared imaging survey such as the CFHT Legacy Survey (CFHTLS; Willott et al. 2010a), Pan-STARRS (Venemans et al. 2015; Tang et al. 2017; Mazzucchelli et al. 2017), the Dark Energy Survey (DES; Reed et al. 2017, 2019; Yang et al. 2019), the Dark Energy Spectro-

scopic Instrument Legacy Imaging Surveys (DELS; Wang et al. 2017, 2018b,a), the Subaru HSC-SSP survey (Matsuoka et al. 2016, 2018a,b, 2019), VISTA (Venemans et al. 2013; Pons et al. 2019) and the UKIRT InfraRed Deep Sky Surveys-Large Area Survey (ULAS; Mortlock et al. 2011; Bañados et al. 2018a).

X-ray observations are a very powerful tool to understand quasars providing information on the region close to the central SMBH. However only two $z > 6.5$ quasars have published observation at X-rays; ULAS J1120+0641 at $z = 7.1$ Page et al. (2014) and ULAS J1342+0928 at $z = 7.5$ Bañados et al. (2018b). X-ray studies of high-redshift ($z \sim 6$) quasars have shown that their optical and X-ray properties are similar to those of low redshift quasars with similar average X-ray spectral photon index (see for example Farrah et al. 2004; Page et al. 2005; Nanni et al. 2017) and comparable luminosity at $\lambda = 2500\text{\AA}$. Also, no dependence of the optical-to-X-ray slope (α_{ox}) with redshift have been found

* E-mail: epons@ast.cam.ac.uk

Table 1. XMM observations log for the DES and new $z > 6.4$ X-ray quasars

Object	R.A.	Dec	z	$N_{H,Gal}$ (10^{20} cm^{-2})	Obs. Date	t_{exp}^a (ks)	XMM OBSID	PI	Ref ^b
VDES J0020–3653	5.13113	-36.89494	6.834	1.53	2018 May 14	24.8	0824400101	Pons E.	2/2
VDES J0244–5008	41.00425	-50.14825	6.724	2.55	2018 May 16	17.0	0824400201	Pons E.	2/2
VDES J0224–4711	36.11058	-47.19149	6.526	1.66	2018 May 25	26.1	0824400301	Pons E.	1/2
PSO J338.2298+29.5089	338.22975	29.50897	6.658	6.17	2017 Nov. 26	23.7	0803160301	Schartel N.	4/4
VIK J0109–3047	17.47138	-30.79064	6.747	2.32	2017 Dec. 06	6.0	0803160201	Schartel N.	3/8
PSO J159.2257–02.5438	159.22579	-2.54386	6.38	4.74	2017 Dec. 22	19.9	0803161101	Schartel N.	5/5
VIK J0305–3150	46.32050	-31.84886	6.605	1.42	2018 Jan. 05	22.0	0803160401	Schartel N.	3/8
PSO J036.5078+03.0498	36.50779	3.04983	6.541	3.04	2018 Jan. 16	16.8	0803160501	Schartel N.	4/4
CFHQS J0210–0456	32.55496	-4.93914	6.438	1.88	2018 Feb. 02	8.4	0803160701	Schartel N.	6/7

^a EPIC net exposure times after high particle background filtering. Mean between the pn and MOS detectors.

^b Discovery / redshift references: (1) Reed et al. (2017), (2) Reed et al. (2019), (3) Venemans et al. (2013), (4) Venemans et al. (2015), (5) Bañados et al. (2016), (6) Willott et al. (2010a), (7) Willott et al. (2010b) and (8) De Rosa et al. (2014).

up to $z \sim 6$ (Brandt et al. 2002; Steffen et al. 2006) - the apparent correlation being only an artifact from the dependence of $L_{2500\text{\AA}}$ with the redshift (Steffen et al. 2006; Lusso et al. 2010) - suggesting that the central X-ray energy source of quasars does not evolve strongly over cosmic time. Furthermore, previous work (Steffen et al. 2006; Lusso et al. 2010) has found evidence that α_{ox} anti-correlates with the quasar UV luminosity $L_{2500\text{\AA}}$, with more luminous quasars having more negative values of α_{ox} (i.e. α_{ox} i.e. relative less X-ray emission as $L_{2500\text{\AA}}$ increases). This indicates that for powerful quasars the X-ray emission produced by the hot corona is weaker relative to the UV and optical emission from the disk.

In order to improve our knowledge of the X-ray properties of $z > 6.5$ quasars, in this paper we report *XMM-Newton* observations and analysis of a sample of nine quasars with $z \gtrsim 6.5$; three quasars from the Dark Energy Survey (DES) at $z > 6.5$, VDES J0020–3653 ($z = 6.824$), VDES J0244–5008 ($z = 6.724$) VDES J0224–4711 ($z = 6.526$) and of six other quasars with $6.438 < z < 6.747$ from the *XMM-Newton* public archive in Section 2. The data analysis of these sources is presented in Section 3 and finally in Section 4, we discuss the X-ray and optical properties of the nine quasars in our sample compared to previous X-ray observations of high-redshift quasars. We assume a flat cosmology with $H_0 = 70 \text{ km s}^{-1}$, $\Omega_M = 0.3$ and $\Omega_\Lambda = 0.7$.

2 XMM OBSERVATIONS AND DATA REDUCTION

In this paper we present the *XMM-Newton* of three spectroscopically confirmed high-redshift ($z > 6.5$) quasars recently discovered using observations from the Dark Energy Survey (DES) Reed et al. (2017, 2019) though colour selection and spectral energy distribution fitting of DES optical, VISTA near-infrared and WISE mid-infrared photometry. *XMM-Newton* observing time were allocated through the call of proposal for period AO-17, and they were observed in 2018 May with 28.3ks, 28.0ks and 35.9ks exposure for VDES J0020–3653, VDES J0244–5008 and VDES J0224–4711 respectively. In addition we present the analysis of six other quasars with $6.44 < z < 6.75$ with X-ray observations in

the *XMM-Newton* public archive. These six quasars were also selected from wide field optical and near-IR surveys i.e. CFHTLS (Willott et al. 2010a), Pan-STARRS1 (Bañados et al. 2016; Venemans et al. 2015) and VISTA VIKING (Venemans et al. 2013). They have been observed between 2017 November and 2018 February for a total observing time of 23 to 33ks. The redshifts as well as the X-ray observations log for the full sample of 9 $z \gtrsim 6.4$ quasars are reported in Table 1 and J-band continuum magnitudes are given in Table 4.

The X-ray observational data were obtained with the European Photon Imaging Camera (EPIC; Strüder et al. 2001; Turner et al. 2001), which consists of one pn and two MOS cameras, and was operated in full-frame mode with thin filters for all the observations. The data were processed using the standard *XMM-Newton Science Analysis Software* (SAS) with version 17.0.0. We excluded time intervals affected by high particle background through inspection of the light curves in the 10–12 keV energy range, resulting of net exposure times between 17.0 and 26ks (see Table 1). To construct events files we used the standard EPIC events pattern selection; i.e. 0–12 and 0–4 for MOS and pn respectively. We then produced images in five energy bands: 0.2–10, 0.2–0.5, 0.5–2.0, 2.0–5.0 and 5.0–10.0 keV.

To check if the sources were detected and measure the X-ray flux, we performed a simultaneous EPIC (pn+MOS) sources detection in each band using the SAS task `edetect_chain` with a detection likelihood threshold of 10 (corresponding to 4σ). We also used the SAS task `eregionanalyse` to compute fluxes or perform 3σ upper limit estimations in each energy bands on the pn and MOS images, by extracting the number of counts in a circular region of $10''$ radius. To get an accurate estimation of the number of counts, we used the exposure map created by the `edetect_chain` task and we selected a background circular region adjacent to the target and on the same chip, free of sources, with a larger radius.

In order to convert the count rates to flux for our different energy ranges and detectors, we computed energy conversion factors (ecf) using WebPIMMS, converting from a XMM-MOS/pn thin count rate to a flux assuming a power-law spectral shape with a slope of 1.9 modified by galactic absorption. The EPIC parameters (i.e. source counts, count

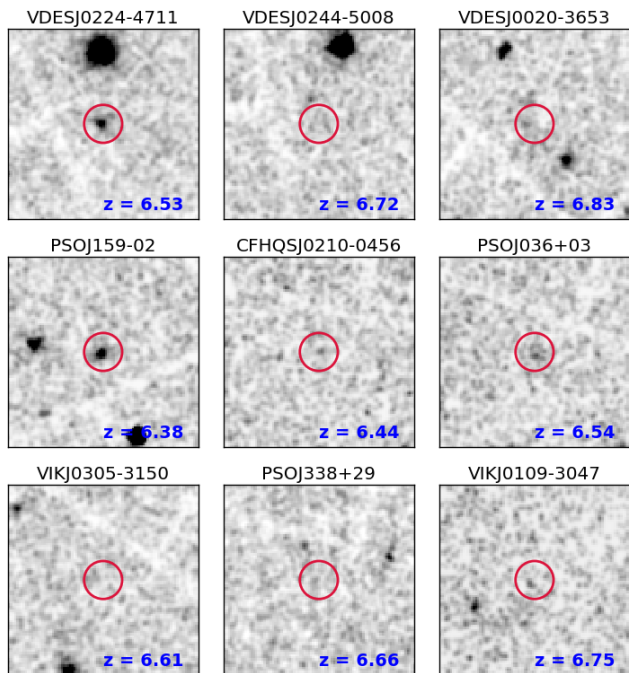


Figure 1. Full band (0.2–10 keV) EPIC 100'' mosaics for the three DES $z > 6.5$ quasars (top row) and 6 newly analysed $z > 6.4$ quasars. Red circles are 10'' radius, which correspond to the extraction radius. The images has been smoothed with a Gaussian function of $\sigma = 1.0$ pixel.

rates and fluxes, HR) correspond to the weighted mean of the values obtained for the pn, MOS1 and MOS2 cameras. When the resulting flux values are smaller than their 3σ errors the 3σ upper limits are given.

In the case where an X-ray source is detected at greater than 4σ (i.e. VDES J0224–4711 and PSO J159–02, see Section 3), we extracted a spectrum from a 15''/11'' radius region around the target position in the pn/MOS detectors. The background spectrum was extracted on the same region that the one used by the `eregionanalyse` task. We then combined the pn and MOS spectra into a single EPIC spectrum using the `epicspeccombine`, with corresponding background spectra and response matrix also combined. For the resulting EPIC spectra, we grouped the data with only one count per bin, due to low number of counts.

3 RESULTS

From our three DES targets, only one has been clearly detected in the X-rays: VDES J0224–4711. Its detected net counts in the full 0.2–10 keV energy range is 174, corresponding to a flux of $\sim 12 \times 10^{-15}$ erg cm $^{-2}$ s $^{-1}$ with a detection significance of 9σ ; the X-ray source is clearly visible on the image Figure 1. It is also detected individually in the 0.5–2.0 keV energy range with 118 net counts and a detection significance of 8σ (see Table 2). The separation between the optical position of this quasar and the *XMM* detection is only 2.52'', with the uncertainty on the X-ray position being less than 1'' ($\sim 0.81''$).

The two other DES quasars, VDES J0244–5008

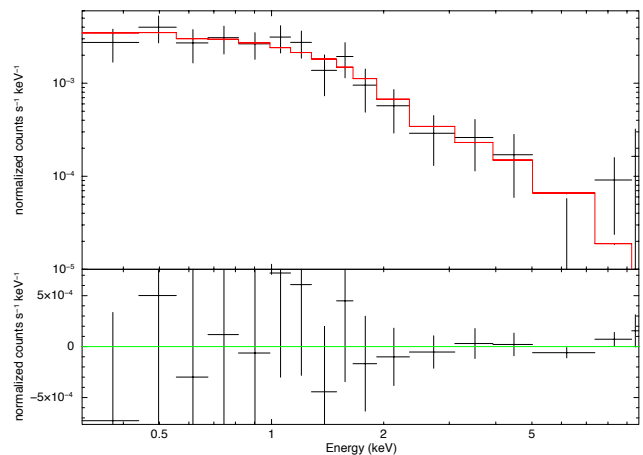


Figure 2. Upper panel: *XMM-Newton* spectrum of VDES J0224–4711. The fit with a power law component modified by Galactic absorption is shown by the red line. Lower panel: Residuals between the data and the best fit model. For a better visualisation adjacent bins have been combined until they have a significant detection of at least 20σ (`XSPEC rebin` command). This is for plotting purpose only and has no influence on the fit.

and VDES J0020–3653, are not detected using the `edetect_chain` task. From the `eregionanalyse` task, VDES J0020–3653 have about 100 net counts in the 0.2–10keV energy range, corresponding to a flux of $\sim 6 \times 10^{-15}$ erg cm $^{-2}$ s $^{-1}$. Finally, VDES J0244–5008 have only 45 counts in the full energy range and a flux of $\sim 5 \times 10^{-15}$ erg cm $^{-2}$ s $^{-1}$.

The EPIC spectrum for VDES J0224–4711 is shown in Figure 2. We fit it using `XSPEC` with a single power-law model (`zpo`) modified by Galactic absorption (`tbabs`). Due to the low number of counts, we used the Cash statistic `Cash` (1979). With the Galaxy absorption component kept fix, we found a photon index on $\Gamma = 1.82^{+0.29}_{-0.27}$ with C – stat = 135.5 for 161 degrees of freedom and get a flux in the 2–10keV energy range of $f_{2-10keV} = (7.38 \pm 1.09) \times 10^{-15}$ erg cm $^{-2}$ s $^{-1}$. Such a value of Γ is consistent with what is observed for quasars in the low (Page et al. 2005; Piconcelli et al. 2005; Just et al. 2007) and high (Shemmer et al. 2005; Nanni et al. 2017) redshift Universe.

For the three DES quasars, the EPIC net source counts (i.e. after background subtraction) and fluxes in the full (0.2–10 keV) energy range in in the 0.2–0.5, 0.5–2.0, 2.0–5.0 and 5.0–10.0 keV energy ranges are given in Table 2. The full band *XMM* 100'' EPIC mosaic of the DES $z > 6.5$ quasars are shown in Figure 1 (top row).

Among the six other quasars, only PSO J159.2257–02.5438 ($z = 6.38$) has been detected with 127 counts in the 0.2–10 keV band, corresponding to a flux of $\sim 11 \times 10^{-15}$ erg cm $^{-2}$ s $^{-1}$, and a detection significance of 8σ . It is also detected individually in the 0.5–2.0 keV and 2.0–5.0 keV energy bands with 84 counts (7σ significance) and 27 counts (4σ significance) respectively. As for VDES J0224–4711, the separation between the optical and X-ray positions is quite small ($\sim 1.30''$) and the error on the *XMM* position is only 0.83''. From fitting its spectrum with a single power-law modified by Galactic absorption,

Table 2. X-ray net counts and fluxes for the DES quasars

Energy range	Net counts	Flux (10^{-15} erg cm $^{-2}$ s $^{-1}$)	Det.
VDES J0224–4711 ($z = 6.526$)			
0.2 - 10 keV	173.3 ± 20.3	11.96 ± 1.39	9σ
0.2 - 0.5 keV	< 23.8	< 1.76	
0.5 - 2.0 keV	118.1 ± 15.4	5.08 ± 0.65	8σ
2.0 - 5.0 keV	29.2 ± 8.8	3.83 ± 1.16	
5.0 - 10 keV	< 16.5	< 22.48	
VDES J0244–5008 ($z = 6.724$)			
0.2 - 10 keV	< 34.6	< 8.8	
0.2 - 0.5 keV	< 13.6	< 2.71	
0.5 - 2.0 keV	< 24.0	< 4.50	
2.0 - 5.0 keV	< 7.1	< 6.49	
5.0 - 10 keV	< 4.1	< 31.41	
VDES J0020–3653 ($z = 6.834$)			
0.2 - 10 keV	36.0 ± 11.7	2.68 ± 0.87	
0.2 - 0.5 keV	< 18.2	< 2.13	
0.5 - 2.0 keV	< 26.0	< 2.39	
2.0 - 5.0 keV	< 5.6	< 5.47	
5.0 - 10 keV	< 14.1	< 24.86	

Note: The upper limits quoted in this table correspond to the 3σ upper limits and are used only if the nets counts or fluxes are smaller than their σ error. But only the quasars with a given value in the "Det" column have an X-ray detection.

we get a photon index of $\Gamma = 1.94^{+0.31}_{-0.29}$ (C-stat = 117.2 for 115 degrees of freedom), similar to what we found for VDES J0224–4711, and we obtained a 2–10 keV flux of $f_{2-10\text{keV}} = (5.52 \pm 1.72) \times 10^{-15}$ erg cm $^{-2}$ s $^{-1}$. For the undetected 5 other quasars we provide estimation of the net source counts and fluxes from the `eregionanalyse` task. They have less than 35 counts in the full band, for three of them we even only get upper limits. The EPIC net source counts and fluxes in the full (0.2–10 keV) energy range in in the 0.2–0.5, 0.5–2.0, 2.0–5.0 and 5.0–10.0 keV energy ranges obtained for these quasars are summarised in Table 3. The full band *XMM* 100'' EPIC mosaic of these 6 quasars are shown in Figure 1 (rows 2 and 3).

For the two X-ray detected quasars in this work, the source counts and fluxes presented in Tables 2 and 3 are from the `edetect_chain` task.

4 DISCUSSION

For the full sample of nine quasars we derived a set of optical and X-ray properties (see Table 4):

- The absolute magnitude at the rest-frame wavelength of $\lambda = 1450\text{\AA}$ (M_{1450}) was computed by extrapolating the J-band magnitude to the monochromatic magnitude at $\lambda = 1450\text{\AA}$ (m_{1450}) assuming a power-law fit of the continuum in the UV-optical $f_\nu \propto \nu^{\alpha_\nu}$ with $\alpha_\nu = -0.3$ (Selsing et al. 2016).

- The monochromatic flux at the rest-frame wavelength of 2500\AA ($f_{2500\text{\AA}}$) was derived from m_{1450} assuming also a power-law slope of $\alpha_\nu = -0.3$.

- The X-ray luminosity in the rest-frame 2-10 keV band was computed from the count rate obtained by the

Table 3. X-ray net counts and fluxes for the new $z > 6.4$ X-ray quasars

Energy range	Net counts	Flux (10^{-15} erg cm $^{-2}$ s $^{-1}$)	Det.
PSO J159.2257–02.5438 ($z = 6.38$)			
0.2 - 10 keV	127.1 ± 15.8	10.82 ± 1.35	8σ
0.2 - 0.5 keV	< 24.4	< 4.4	
0.5 - 2.0 keV	83.8 ± 11.8	4.11 ± 0.58	7σ
2.0 - 5.0 keV	26.5 ± 7.2	3.90 ± 1.13	4σ
5.0 - 10 keV	< 8.4	< 26.72	
CFHQS J0210–0456 ($z = 6.438$)			
0.2 - 10 keV	< 16.2	< 14.39	
0.2 - 0.5 keV	< 6.7	< 5.77	
0.5 - 2.0 keV	< 6.1	< 5.53	
2.0 - 5.0 keV	< 2.6	< 11.81	
5.0 - 10 keV	< 11.2	< 77.09	
PSO J036.5078+03.0498 ($z = 6.541$)			
0.2 - 10 keV	40.4 ± 11.4	4.19 ± 2.05	
0.2 - 0.5 keV	< 22.6	< 10.19	
0.5 - 2.0 keV	24.0 ± 7.8	1.43 ± 0.5	
2.0 - 5.0 keV	< 8.9	< 26.84	
5.0 - 10 keV	< 1.6	< 105.23	
VIK J0305–3150 ($z = 6.605$)			
0.2 - 10 keV	< 13.3	< 5.40	
0.2 - 0.5 keV	< 1.9	< 2.04	
0.5 - 2.0 keV	< 13.5	< 2.54	
2.0 - 5.0 keV	< 1.9	< 5.11	
5.0 - 10 keV	< 9.1	< 28.57	
PSO J338.2298+29.5089 ($z = 6.658$)			
0.2 - 10 keV	< 22.6	< 5.89	
0.2 - 0.5 keV	< 9.7	< 2.32	
0.5 - 2.0 keV	< 19.3	< 3.41	
2.0 - 5.0 keV	< 12.5	< 5.02	
5.0 - 10 keV	< 7.1	< 17.02	
VIK J0109–3047 ($z = 6.747$)			
0.2 - 10 keV	< 10.0	< 16.73	
0.2 - 0.5 keV	< 2.6	< 6.03	
0.5 - 2.0 keV	< 10.9	< 6.8	
2.0 - 5.0 keV	< 5.5	< 18.39	
5.0 - 10 keV	< 1.3	< 60.40	

Note: The upper limits quoted in this table correspond to the 3σ upper limits and are used only if the nets counts or fluxes are smaller than their 3σ error. But only the quasars with a given value in the "Det" column have an X-ray detection.

`eregionanalyse` task on the 2-10 keV image (as done in Section 2 for the other energy ranges) and then K-correction was applied assuming a photon index $\Gamma = 1.9$. For the two detected quasars VDES J0224–4711 and PSO J159.2257–02.5438 the flux was obtained directly from their X-ray spectrum. Upper limits are used if the luminosity is smaller than three times its error (which is the case for all the non-detected sources) and are at the 3σ level.

- The hardness ratio is defined as $HR = (H - S)/(H + S)$ where S and H are the number of counts in the soft (0.5–2.0 keV) and hard (2.0–5.0 keV) bands.

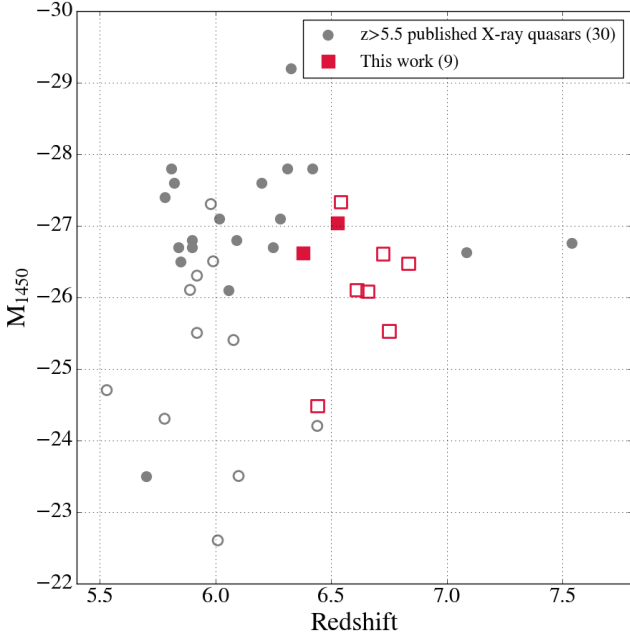


Figure 3. Absolute magnitude M_{1450} versus redshift of all the X-ray observed quasars at $z > 5.5$, including our three quasars from DES (red squares), the newly observed Pan-STARRS quasars by N. Schartel (blue diamonds) and the published quasars as compiled by Nanni et al. (2017) plus those by Nanni et al. (2018) and Bañados et al. (2018b) (grey circles). The open symbols correspond to undetected X-ray sources and filled symbols are for quasars detected in the X-rays. The new sample from this work allows to fill the gap of X-ray observed quasars between $6.4 < z < 7.0$

– The optical-to-X-ray slope (α_{ox}) is defined as

$$\alpha_{ox} = 0.3838 \times \log \left(\frac{f_{2\text{keV}}}{f_{2500\text{\AA}}} \right) \quad (1)$$

where $f_{2500\text{\AA}}$ is the monochromatic flux at the rest-frame wavelength of 2500\AA as defined above and the rest-frame monochromatic flux at 2 keV ($f_{2\text{keV}}$) was inferred from the flux in the 0.2–10 keV range assuming a photon index $\Gamma = 1.9$. Upper-limits for α_{ox} are used if the flux at 2 keV is smaller than three times its error.

We used the compilation of X-ray observations of quasars at $z > 5.5$ by Nanni et al. (2017) plus the new analysis by Nanni et al. (2018) for SDSS J1030+0524 ($z=6.28$) and the observation of ULAS J1342+0928 ($z=7.54$) by Bañados et al. (2018b) to compare with the properties of our new sample. This new sample allows us to fill the gap between $6.4 < z < 7.0$ of observed high-redshift quasars in the X-rays.

The magnitude M_{1450} versus redshift distribution of the X-ray observed $z > 5.5$ quasars is shown in Figure 3. The median absolute magnitude at $\lambda = 1450\text{\AA}$ is $M_{1450} = -26.1$ for the nine newly observed quasars, which is similar to the median value ($M_{1450} = -26.7$) for the sample of previously known $z > 5.5$ quasars including the two quasars at $z > 7.0$. Only one quasar with $M_{1450} > -25$ has been previously detected in the X-rays (RD J1148+5253, $z = 5.7$;

Gallerani et al. 2017). This quasar was a serendipitous detection in the 78ks *Chandra* observation of the $z = 6.4$ quasar SDSSJ1148+5251. It has about 4 times more exposure time than the other X-ray detected high-redshift quasars, and only ~ 3 counts were detected. For comparison, the lowest UV luminosity source in our sample, CFHQS J0210–0456 ($M_{1450} = 24.98$), has an upper limit of 14 counts in the 0.2–10 keV band.

For the two X-ray detected quasars, we found that their X-ray spectra are well fitted with a standard AGN model which consists of a power-law modified by Galactic absorption. The power-law has a photon index $\Gamma \sim 1.9$ which is consistent with value observed at $z \sim 6$ quasars by Nanni et al. (2017) and also with lower redshift quasars, as firstly observed by Nandra et al. (1997). Another indicator of the X-ray spectral shape is the hardness ratio. In the absence of obscuration low and high redshift quasars should appear soft in the X-rays and are expected to have a low hardness ratio with $HR \sim -0.5$ (Wang et al. 2004). For the sources with enough counts we obtained a hardness ratio $HR \sim -0.55$ (see Table 4), similar to what is expected for high-redshift quasars and also what have been observed in $z \sim 6$ quasars Nanni et al. (2017).

On the left panel of Figure 4 we show the X-ray luminosity in the rest-frame 2–10 keV band ($L_{2-10\text{keV}}$). The new detected sources in our work are amongst the most luminous X-ray quasars at $z > 5.5$ with $L_{2-10\text{keV}} \sim 2-4 \times 10^{45}$ erg s^{-1} . VDES J0224–4711 which is the only DES quasar detected in the X-rays has a rest-frame 2–10 keV luminosity of $L_{2-10\text{keV}} = (2.92 \pm 0.43) \times 10^{45}$ erg s^{-1} , 6 times and 2.5 times larger than the ULAS J1120+0641 ($z = 7.08$) and ULAS J1342+0928 ($z = 7.54$) respectively. The only other quasar detected is PSO J159–02 with $L_{2-10\text{keV}} = (2.08 \pm 0.65) \times 10^{45}$ erg s^{-1} , i.e. a value similar to VDES J0224–4711. The other quasars have upper limits in their X-ray luminosity with $L_{2-10\text{keV}} < 2 \times 10^{46}$ erg s^{-1} .

The optical-to-X-ray slope α_{ox} computed for the quasars in our sample is consistent with the observed $\alpha_{ox} - L_{2500\text{\AA}}$ correlation inferred by Nanni et al. (2017) who added 29 quasars with $z > 5.5$ to the a sample of a thousand lower redshift quasars (see the right panel of Figure 4). These luminous quasars at $z > 6.4$ follow the trend of decreasing α_{ox} as $L_{2500\text{\AA}}$ increases, as found in previous studies (Steffen et al. 2006; Lusso et al. 2010) for quasars at lower redshift. To be consistent we re-computed the α_{ox} and $L_{2500\text{\AA}}$ from Nanni et al. (2017) assuming a power-law slope in the UV-optical of $\alpha_{\nu} = -0.3$ (while $\alpha_{\nu} = -0.5$ is used by Nanni et al. (2017)). Changing the slope only has a small effect, as $L_{2500\text{\AA}}$ increases by $\sim 10\%$ and α_{ox} is larger by 0.018.

Previous studies of α_{ox} in quasars (Strateva et al. 2005; Shemmer et al. 2005; Just et al. 2007; Lusso et al. 2010) have tested for possible redshift dependence of α_{ox} but they did not find any significant correlation between the two. The apparent correlation between α_{ox} and the redshift (i.e. α_{ox} seems to decrease as the redshift increases from $z \sim 0$ up to $z \sim 6$) for quasars with broad range of luminosity $10^{27} < L_{2500\text{\AA}} < 10^{33}$ erg s^{-1} Hz is in fact only an artifact due to the effect of the optical luminosity. The X-ray quasars at $z > 5.5$ span a narrower range of optical luminosity ($10^{30} < L_{2500\text{\AA}} < 10^{33}$ erg s^{-1} Hz) and we do not observe any obvious evolution of α_{ox} with redshift (see Fig-

Table 4. Summary of X-ray and optical properties of the DES and new $z > 6.4$ X-ray quasars

Object	z	J_{AB}	M_{1450}	$f_{2500\text{\AA}}^{\circ}$ (10^{-28} erg cm $^{-2}$ s $^{-1}$ Hz $^{-1}$)	$L_{2-10\text{keV}}$ (10^{45} erg s $^{-1}$)	HR	α_{ox}^a
VDES J0224–4711	6.526	19.75 ± 0.06	-27.03	5.17 ± 0.29	2.92 ± 0.43	-0.56 ± 0.11	-1.95 ± 0.03
VDES J0244–5008	6.724	20.23 ± 0.13	-26.61	3.34 ± 0.38	< 4.37	–	< -1.89
VDES J0020–3653	6.834	20.4 ± 0.10	-26.47	2.88 ± 0.26	< 4.76	–	-2.07 ± 0.07
PSO J159–02	6.38	20.13 ± 0.05	-26.62	3.64 ± 0.16	2.59 ± 0.82	-0.52 ± 0.12	-1.88 ± 0.03
CFHQS J0210–0456	6.438	22.28 ± 0.27	-24.98	0.50 ± 0.11	< 10.00	–	< -1.49
PSO J036+03	6.541	19.46 ± 0.10	-27.33	6.78 ± 0.60	< 17.62	-0.58 ± 0.36	-2.13 ± 0.06
VIK J0305–3150	6.605	20.71 ± 0.09	-26.10	2.15 ± 0.18	< 4.28	–	< -1.90
PSO J338+29	6.658	20.74 ± 0.09	-26.08	2.09 ± 0.17	< 3.80	–	< -1.88
VIK J0109–3047	6.747	21.32 ± 0.14	-25.53	1.23 ± 0.15	< 12.59	–	< -1.62

^a Reminder: A non-upper limit on the α_{ox} slope does not imply a significant detection. Only VDES J0224–4711 and PSO J159–02 are detected in the X-rays. Upper-limits are used only if the flux at 2keV is smaller than its 3σ error.

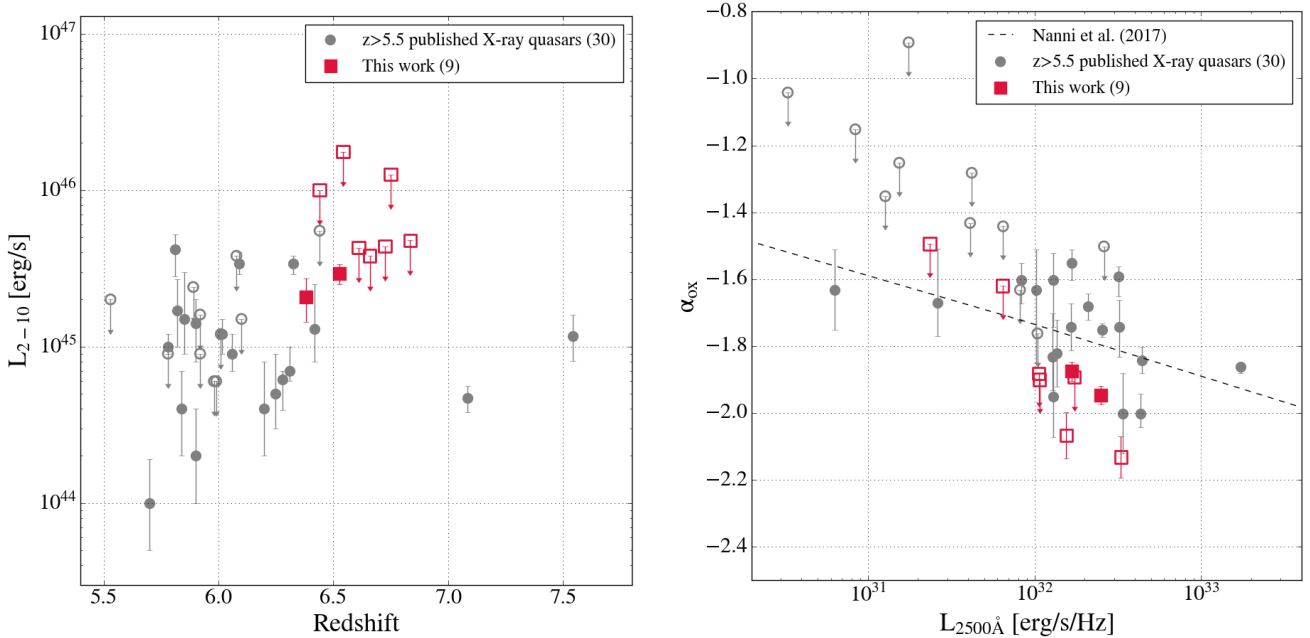


Figure 4. X-ray and optical properties of all the X-ray observed quasars at $z > 5.5$. For a description of symbols see Figure 3. *Left panel:* X-ray luminosity in the rest-frame 2–10 keV band $L_{2-10\text{keV}}$ versus redshift. The two detected new quasars from this work have an X-ray luminosity in the upper range of the distribution of $L_{2-10\text{keV}}$ for $z > 5.5$ quasars, with an X-ray luminosity 6 times larger than ULAS J1120+0641 ($z = 7.08$). *Right panel:* Correlation between the optical-to-X-ray slope α_{ox} and the luminosity at the rest-frame $\lambda = 2500\text{\AA}$ ($L_{2500\text{\AA}}^{\circ}$). The dashed line corresponds to the best fit relation from Nanni et al. (2017), and the quasars from this work are broadly consistent with this expectation. **Note:** A non-upper limit on the α_{ox} slope does not imply a detection, only the filled symbols correspond to significant (4σ) detections.

ure 5; top panel), especially when correcting for the effect of the luminosity (see Figure 5; bottom panel).

5 CONCLUSION

We present *XMM-Newton* X-ray observations and analysis of three $z > 6.5$ quasars previously discovered in the Dark Energy Survey and the X-ray analysis of six other quasars with $6.438 < z < 6.747$ from the *XMM-Newton* public archive. The analysis of these sources show that two quasars VDES J0224–4711 ($z = 6.526$) and PSO J159–02 ($z = 6.38$) are detected in the X-rays 0.2–10 keV energy

band. VDES J0224–4711 is detected with a significance of 9σ and ~ 174 net counts corresponding to a flux of $f_{2-10\text{keV}} \sim 12 \times 10^{-15}$ erg cm $^{-2}$ s $^{-1}$. PSO J159–02 is detected with a significance of 8σ , and ~ 127 net counts, corresponding to a flux of $f_{2-10\text{keV}} \sim 11 \times 10^{-15}$ erg cm $^{-2}$ s $^{-1}$.

VDES J0224–4711 is also detected individually in the 0.5–2.0 keV soft band and PSO J159–02 has individual detection in both the 0.5–2.0 keV and 2.0–5.0 keV bands. The X-ray spectra are well fitted with a power-law with a photon index $\Gamma \sim 1.82_{-0.27}^{+0.29}$ and $\Gamma \sim 1.94_{-0.29}^{+0.31}$ respectively, similarly to what is observed in other quasars at lower redshifts (Nanni et al. 2017). For the seven other quasars undetected in the X-ray (i.e. detection significance $< 4\sigma$) we were still

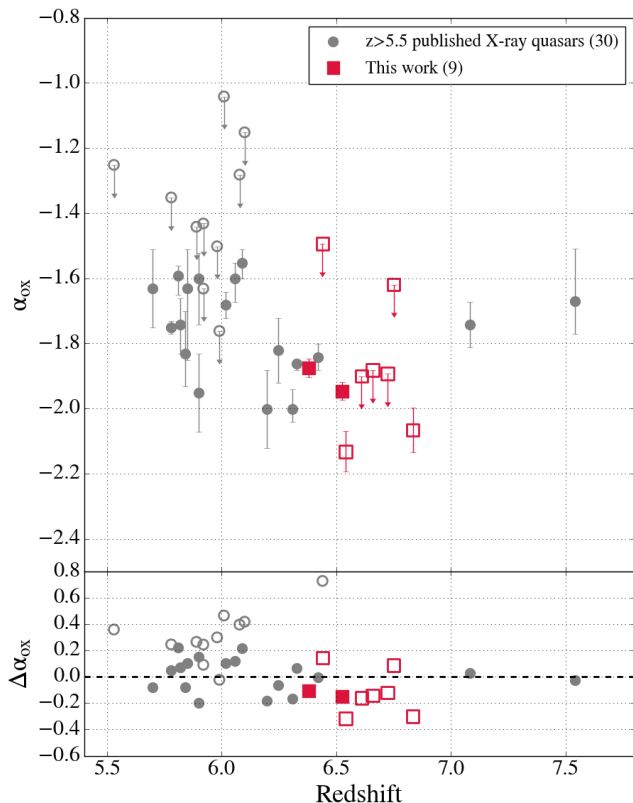


Figure 5. *Top panel:* Optical-to-X-ray slope α_{ox} versus redshift. For a description of the symbols see Figure 3. *Bottom panel:* Difference between the computed α_{ox} and the predicted α_{ox} from $L_{2500\text{\AA}}$ using the correlation by Nanni et al. (2017) ($\Delta\alpha_{ox}$). We do not observe obvious correlation between α_{ox} and the redshift as stated by previous works.

able to estimate X-ray fluxes (or 3σ upper limits) by extracting the number of counts in a circular region around the source position.

The X-ray observations of these 9 quasars allow us to fill the gap in the redshift distribution of high redshift quasars observed in the X-rays for $6.5 < z < 7.0$. Prior to this work, only two quasars ULAS J1120+0641 and ULAS J1342+0928 had X-ray observations among the known quasars at $z > 6.5$. We find that the quasars in our sample have similar M_{1450} magnitudes compared to X-ray observed quasars at $z > 5.5$ with the exception of CFHQS J0210–0456 which has one of the faintest magnitudes ($M_{1450} \sim -24.5$). Furthermore, for the quasars with discrete measurements of $L_{2-10\text{keV}}$, we find that they are among the brightest X-ray quasars at $z > 5.5$ with $L_{2-10\text{keV}} \sim 2 - 4 \times 10^{45} \text{ erg s}^{-1}$, with VDES J0224–4711 and PSO J159–02 - the two quasars with clear X-ray detections - being 6 times and 2.5 times larger than the ULAS J1120+0641 ($z = 7.08$) and ULAS J1342+0928 ($z = 7.54$). Finally the optical-to-X-ray slope α_{ox} we get for the quasars in our sample is consistent with the $\alpha_{ox} - L_{2500\text{\AA}}$ anti-correlation inferred by Nanni et al. (2017) based on low and high-redshift quasars.

ACKNOWLEDGEMENTS

EP, RGM acknowledge the support of UK Science and Technology research Council (STFC). RGM also acknowledges support by ERC Advanced Grant 320596 *The Emergence of Structure during the Epoch of reionization*. This work was made possible thanks to observations obtained with XMM-Newton, an ESA science mission with instruments and contributions directly funded by ESA Member States and NASA.

REFERENCES

- Alexander T., Natarajan P., 2014, *Science*, **345**, 1330
 Bañados E., et al., 2016, *ApJS*, **227**, 11
 Bañados E., et al., 2018a, *Nature*, **553**, 473
 Bañados E., et al., 2018b, *ApJ*, **856**, L25
 Brandt W. N., et al., 2002, *ApJ*, **569**, L5
 Cash W., 1979, *ApJ*, **228**, 939
 De Rosa G., et al., 2014, *ApJ*, **790**, 145
 Farrah D., Priddey R., Wilman R., Haehnelt M., McMahon R., 2004, *ApJ*, **611**, L13
 Gallerani S., et al., 2017, *MNRAS*, **467**, 3590
 Just D. W., Brandt W. N., Shemmer O., Steffen A. T., Schneider D. P., Chartas G., Garmire G. P., 2007, *ApJ*, **665**, 1004
 Lusso E., et al., 2010, *A&A*, **512**, A34
 Matsuoka Y., et al., 2016, *ApJ*, **828**, 26
 Matsuoka Y., et al., 2018a, *PASJ*, **70**, S35
 Matsuoka Y., et al., 2018b, *ApJ*, **869**, 150
 Matsuoka Y., et al., 2019, *ApJ*, **872**, L2
 Mazzucchelli C., et al., 2017, *ApJ*, **849**, 91
 Mortlock D. J., et al., 2011, *Nature*, **474**, 616
 Nandra K., George I. M., Mushotzky R. F., Turner T. J., Yaqoob T., 1997, *ApJ*, **477**, 602
 Nanni R., Vignali C., Gilli R., Moretti A., Brandt W. N., 2017, *A&A*, **603**, A128
 Nanni R., et al., 2018, *A&A*, **614**, A121
 Page K. L., Reeves J. N., O’Brien P. T., Turner M. J. L., 2005, *MNRAS*, **364**, 195
 Page M. J., Simpson C., Mortlock D. J., Warren S. J., Hewett P. C., Venemans B. P., McMahon R. G., 2014, *MNRAS*, **440**, L91
 Piconcelli E., Jimenez-Bailón E., Guainazzi M., Schartel N., Rodríguez-Pascual P. M., Santos-Lleó M., 2005, *A&A*, **432**, 15
 Pons E., McMahon R. G., Simcoe R. A., Banerji M., Hewett P. C., Reed S. L., 2019, *MNRAS*, **484**, 5142
 Reed S. L., et al., 2017, *MNRAS*, **468**, 4702
 Reed S. L., et al., 2019, *MNRAS*, **487**, 1874
 Selsing J., Fynbo J. P. U., Christensen L., Krogager J. K., 2016, *A&A*, **585**, A87
 Shemmer O., Brandt W. N., Vignali C., Schneider D. P., Fan X., Richards G. T., Strauss M. A., 2005, *ApJ*, **630**, 729
 Steffen A. T., Strateva I., Brandt W. N., Alexander D. M., Koekemoer A. M., Lehmer B. D., Schneider D. P., Vignali C., 2006, *AJ*, **131**, 2826
 Strateva I. V., Brandt W. N., Schneider D. P., Vanden Berk D. G., Vignali C., 2005, *AJ*, **130**, 387
 Strüder L., et al., 2001, *A&A*, **365**, L18
 Tang J.-J., et al., 2017, *MNRAS*, **466**, 4568
 Trakhtenbrot B., Volonteri M., Natarajan P., 2017, *ApJ*, **836**, L1
 Turner M. J. L., et al., 2001, *A&A*, **365**, L27
 Venemans B. P., et al., 2013, *ApJ*, **779**, 24
 Venemans B. P., et al., 2015, *ApJ*, **801**, L11
 Volonteri M., 2010, *Astronomy and Astrophysics Review*, **18**, 279

- Wang J. X., Malhotra S., Rhoads J. E., Norman C. A., 2004, *ApJ*, **612**, L109
- Wang F., et al., 2017, *ApJ*, **839**, 27
- Wang F., et al., 2018a, arXiv e-prints, p. [arXiv:1810.11926](https://arxiv.org/abs/1810.11926)
- Wang F., et al., 2018b, *ApJ*, **869**, L9
- Willott C. J., et al., 2010a, *AJ*, **139**, 906
- Willott C. J., et al., 2010b, *AJ*, **140**, 546
- Yang J., et al., 2019, *AJ*, **157**, 236

This paper has been typeset from a $\text{\TeX}/\text{\LaTeX}$ file prepared by the author.